

Topological insulators and fractional quantum Hall effect on the ruby lattice

Xiang Hu,^{*} Mehdi Kargarian, and Gregory A. Fiete

Department of Physics, The University of Texas at Austin, Austin, Texas 78712, USA

(Received 5 June 2011; published 14 October 2011)

We study a tight-binding model on the two-dimensional ruby lattice. This lattice supports several types of first- and second-neighbor spin-dependent hopping parameters in an s -band model that preserves time-reversal symmetry. We discuss the phase diagram of this model for various values of the hopping parameters and filling fractions and note an interesting competition between spin-orbit terms that individually would drive the system to a Z_2 topological insulating phase. We also discuss a closely related spin-polarized model with only first- and second-neighbor hoppings and show that extremely flat bands with finite Chern numbers result, with a ratio of the band gap to the band width of approximately 70. Such flat bands are an ideal platform to realize a fractional quantum Hall effect at appropriate filling fractions. The ruby lattice can be possibly engineered in optical lattices and may open the door to studies of transitions among quantum spin liquids, topological insulators, and integer and fractional quantum Hall states.

DOI: [10.1103/PhysRevB.84.155116](https://doi.org/10.1103/PhysRevB.84.155116)

PACS number(s): 71.10.Fd, 71.10.Pm, 73.20.-r, 73.43.-f

I. INTRODUCTION

Topological phases of matter have received a great deal of attention recently.^{1,2} In part, this is motivated by the fractional quantum Hall effect and its possible role as a platform for topological quantum computation.³ However, there is also a more general interest in phases of quantum many-particle systems that can exhibit responses and other properties that are a consequence of global (i.e., topological) features that are not captured in a local order parameter.⁴⁻⁶ A key example of such a phase is the time-reversal-invariant topological insulator.⁷⁻⁹ In contrast to most of the previously known systems that exhibited some topological property (the integer quantum Hall effect being a notable exception), topological insulators do not require electron-electron interactions, but they are stable to interactions of weak to moderate strength.⁷⁻⁹ The weakly interacting nature of topological insulators has enabled accurate predictions¹⁰⁻¹³ for a wide range of two- and three-dimensional systems,¹⁴⁻²⁸ and experiment has followed with confirming data in a large and rapidly growing number of instances.²⁹⁻⁴⁰

The salient feature of topological insulators is that their boundaries possess a topologically protected “metallic” state that is robust to disorder.⁴¹⁻⁴⁷ Both the two-dimensional⁴⁸⁻⁵⁵ and the three-dimensional⁵⁶⁻⁵⁹ boundaries have been shown to exhibit interesting responses to perturbations. In this work we focus on a two-dimensional tight-binding model with a single s -orbital on each lattice site. We study the so-called ruby lattice shown in Fig. 1. We find that it exhibits a complex phase diagram that includes topological insulators at a number of filling fractions. This lattice has earlier played an important role in the study of topological order in spin models.^{60,61}

Starting with the work of Kane and Mele^{62,63} on the honeycomb lattice (and key earlier precedents by Haldane⁶⁴ in a spinless version), such simple noninteracting lattice models have helped to develop our understanding of topological insulators.⁶⁵ Besides the honeycomb lattice,^{62,63} a number of other two-dimensional lattices have been shown to support a topological insulator phase, including the decorated honeycomb lattice,⁶⁶ the checkerboard lattice,⁶⁷ the square-octagon lattice,⁶⁸ the kagome lattice,⁶⁹ and others.⁷⁰ It is now well

appreciated that such noninteracting lattice models possess topological features that commonly occur in interacting models *without spin-orbit coupling* at the mean-field level.^{67,71-74} Evidently, such simple lattice models contain rather rich physics.

An interesting related topic of study is the class of insulators with nearly flat bands that possess finite Chern numbers. With a finite Chern number, a partial filling of the flat bands can lead to a fractional quantum Hall effect.⁷⁵ To date, only a few lattice models have been proposed which are expected to lead to a fractional quantum Hall effect.⁷⁶⁻⁷⁹ The relevant figure of merit in such models is the ratio of the band gap to the bandwidth of the flat band with a finite Chern number. In the model we discuss in this paper, we find that this ratio can be as high as 70, which is among the largest in the models reported in the literature thus far.

The remainder of the paper is organized as follows. In Sec. II we introduce our tight-binding model, and we discuss the basic features of the energy bands as a function of the hopping parameters. In Sec. III we discuss the phase diagrams at different filling fractions, and in Sec. IV we discuss a closely related spinless (spin-polarized) model with nearly flat bands and finite Chern number. Our main conclusions are given in Sec. V.

II. HAMILTONIAN AND BAND STRUCTURE

We study the Hamiltonian

$$H = H_0 + H_{SO}, \quad (1)$$

where

$$H_0 = -t \sum_{i,j \in \Delta, \sigma} c_{i\sigma}^\dagger c_{j\sigma} - t_1 \sum_{\Delta \rightarrow \Delta, \sigma} c_{i\sigma}^\dagger c_{j\sigma} \quad (2)$$

and

$$H_{SO} = it_2 \sum_{\langle\langle ij \rangle\rangle, \alpha\beta} v_{ij} s_{\alpha\beta}^z c_{i\alpha}^\dagger c_{j\beta} + it_3 \sum_{\langle\langle ij \rangle\rangle, \alpha\beta} v_{ij} s_{\alpha\beta}^z c_{i\alpha}^\dagger c_{j\beta} \quad (3)$$

on the ruby lattice shown in Fig. 1. Here $c_{i\sigma}^\dagger$ and $c_{i\sigma}$ are, respectively, the creation and annihilation operators of an

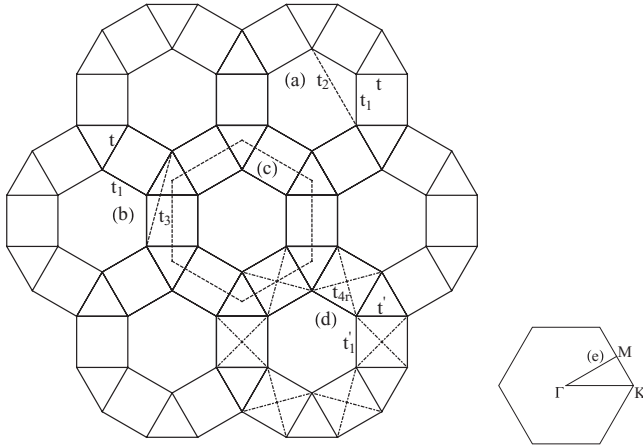


FIG. 1. Schematic of the ruby lattice and illustration of the nearest-neighbor hopping, t, t_1 (real) and t', t'_1 (complex), and the three types of “second-neighbor” spin-orbit coupling or hopping indicated by the dashed or dot dashed lines, t_2, t_3 , and t_{4r} . (a) The spin-orbit coupling strength t_2 within a hexagon. (b) The spin-orbit coupling strength t_3 within a pentagon composed of one triangle and one square. The hoppings t_2 and t_3 are present on all such bonds of the type shown that are consistent with the symmetry of the lattice. (c) The unit cell of the ruby lattice. (d) Schematic of the hopping parameters used to obtain a flat band with a finite Chern number and $W/E_g \approx 70$. (e) The first Brillouin zone of the ruby lattice, with the high symmetry points Γ, M , and K .

electron on site i with spin σ . As indicated in Figs. 1(a) and 1(b), t and t_1 are real first-neighbor hopping parameters, and t_2 and t_3 are real second-neighbor hoppings [which appear with the imaginary number i in Eq. (3), making the total second-neighbor hopping purely imaginary and time-reversal symmetric]. The quantity v_{ij} is equal to 1 if the electron makes a left turn on the lattice links during the second-neighbor hopping, and it is equal to -1 if the electron make a right turn during that process. As is clear from Fig. 1, the unit cell of the lattice contains six sites so six two-fold degenerate bands will result. In addition to the real hopping parameters t and t_1 in (2), symmetry also allows complex, spin-dependent nearest-neighbor hopping with imaginary components t', t'_1 , as shown in Fig. 1. We will discuss terms of this type later in Sec. IV.

The full Hamiltonian (1) can be diagonalized by going to a momentum-space representation:

$$H = \sum_{\mathbf{k}\sigma} \Psi_{\mathbf{k}\sigma}^\dagger \tilde{H}_{\mathbf{k}\sigma} \Psi_{\mathbf{k}\sigma}, \quad (4)$$

where $\Psi_{\mathbf{k}\sigma}^\dagger = (c_{1\mathbf{k}\sigma}^\dagger, c_{2\mathbf{k}\sigma}^\dagger, c_{3\mathbf{k}\sigma}^\dagger, c_{4\mathbf{k}\sigma}^\dagger, c_{5\mathbf{k}\sigma}^\dagger, c_{6\mathbf{k}\sigma}^\dagger)$ is the six-site basis, and $\tilde{H}_{\mathbf{k}\sigma}$ is the Hamiltonian in k space. The bulk energy bands as well as the bands on a strip geometry can be readily calculated. If the problem is solved on a two-dimensional strip, then periodic boundary conditions can be used in one direction (the direction parallel to the length of the strip). We diagonalize the Hamiltonian matrix using standard LAPACK routines.

The bulk energy bands and the energy bands on a strip geometry are shown in Figs. 2 and 3, respectively, for different sets of parameters. Having six sites per unit cell, our tight

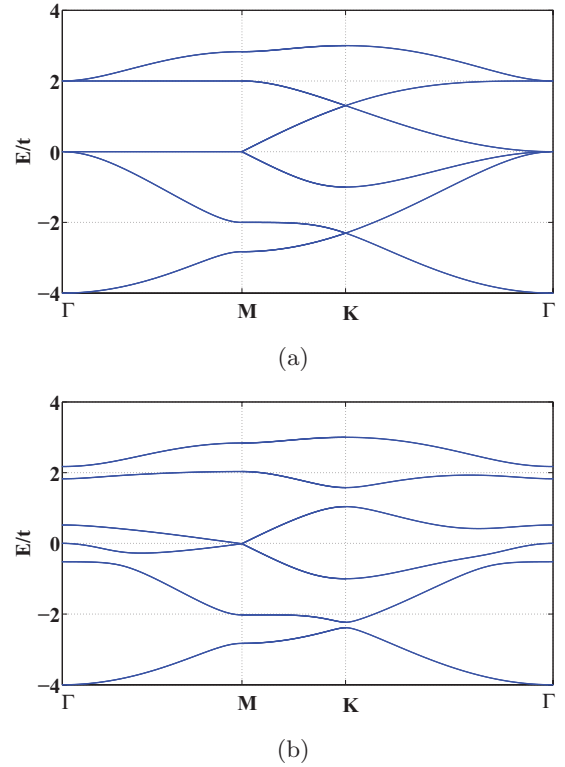


FIG. 2. (Color online) The energy bands without any spin-orbit coupling and with finite spin-orbit coupling, given by Eq. (2). (a) Bulk energy bands along high symmetry directions in the absence of spin-orbit coupling. Note that there is a Dirac point at K for $1/6$ and $2/3$ filling and a quadratic band touching point at Γ for $1/2$ and $5/6$ filling. (The underlying lattice is triangular, as it is for the honeycomb lattice.) Note also the flat bands along the Γ - M direction at $1/2$ and $5/6$ filling. (b) The energy bands for finite spin-orbit coupling, with $t_2 = t_3 = 0.1t$. It is clearly seen that the Dirac points at the K points and quadratic band touching point at the Γ point are removed.

binding model yields six bands that are doubly degenerate due to spin degrees of freedom. Thus the filling factors are determined by counting how many of bands are fully occupied, which are $1/6, 1/3, 1/2, 2/3$, and $5/6$. If one imagines shrinking the triangular plaquettes on the ruby lattice down to a point, the links will look like those of the honeycomb, showing that the underlying Bravais lattice is triangular (since the underlying Bravais lattice of the honeycomb is triangular). For the case $t_1 = t, t_2 = t_3 = 0$ shown in Fig. 2(a) there is no spin-orbit coupling on the lattice, and at all filling fractions the model predicts metallic behavior. Also in Fig. 2(a) we can see that when the energy is zero ($1/2$ filling), three bands are degenerate at the Γ point. For $1/6$ filling and $2/3$ filling, there are Dirac points at the K and K' points. Spin-orbit coupling can open a gap in the spectrum at some fillings [see Fig. 2(b)] and drive the model into an insulator. The nature of these insulators can be further understood by looking at the spectrum of the system with edges, as shown in Fig. 3. We see that at $1/6$ and $2/3$ filling, there exist states at time-reversal-invariant points in k space, that is, at the points where $k_x = 0$ or $k_x = \pi/a$. These states traverse the bulk band gap and are composed of an odd number of Kramers pairs, indicating that the insulating phase is in fact topological.^{62,63}

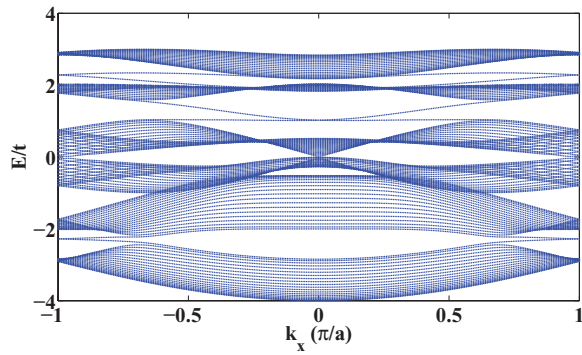


FIG. 3. (Color online) The energy bands on a strip geometry for the case that $t_1 = t$, $t_2 = t_3 = 0.1t$. At filling fractions $1/6$ and $2/3$, edge modes cross the band gap an odd number of times, which clearly reveals the topological insulator phases. Their identification is also confirmed with a direct evaluation of the Z_2 invariant.

A direct evaluation of the Z_2 invariant confirms this, as we will show in the next section. We found that the Dirac point at $2/3$ filling in Fig. 3 is a linear crossing point, but for the special case of $t_1 = t$, $t_2 = 0$, and $-0.04t < t_3 < 0.04t$, the absolute value of the slope at $k_x = 0$ is less than 10^{-4} . Therefore, in an experimental situation where temperature is finite (providing a low-energy cutoff) it could be regarded as a quadratic crossing point. We also verified that a staggered potential with a magnitude as small as $0.01t$ which breaks the C_4 symmetry in the square plaquettes can enhance the slope by one order of magnitude. Our calculation is consistent with the discovery that extra symmetry of the underlying lattice may deform the shape of the Dirac node on the surface of three-dimensional topological insulators, giving rise to a warping effect⁸⁰ or a quadratic crossing in crystalline topological insulators.⁸¹ The flat crossing at $2/3$ filling in our model may alter the low-energy description of the edge modes and change their stability.⁶⁷ In particular, this may make them more susceptible to magnetic ordering from Coulomb interactions.

Having established that our model supports the topological insulator phase, we now turn to cases which explore the whole parameter space of the model and determine the phase diagrams at various filling fractions.

III. PHASE DIAGRAMS OF THE MODEL

We are interested in determining the phases of the Hamiltonian (1) as a function of filling fraction and the hopping parameters t , t_1 , t_2 , and t_3 . From earlier work^{62,63,66–70} we know that we must consider three possible phases: (i) conductor, (ii) insulator, and (iii) topological insulator.

We determine the phase for a given set of parameters in the following way. First we must determine whether the system is conducting or insulating. After choosing a filling fraction, we search for the bottom of the “upper band” with respect to this filling fraction and the top of the “lower band.” For example, at $1/2$ filling the “upper band” would be band 4 and the “lower band” would be band 3, with the labeling starting at the lowest energy band and the counting increasing as one moves to higher energy bands. Finding the extrema of a given energy band is a formidable task since the band structure is rather complex and there are many local minima and maxima. We

use an optimization algorithm called the differential evolution method.⁸² The method works well in most cases, but is not so efficient for some special parameters. In those cases, we use the software MATHEMATICA to help us to determine the extreme values. If the system is insulating (i.e., there is a positive gap between the “upper band” minimum and the “lower band” maximum), then we calculate the Z_2 invariant according to the scheme proposed by Fu and Kane.¹¹

By taking the real-space triangular Bravais vectors of the ruby lattice as $\mathbf{a}_1 = a\hat{x}$ and $\mathbf{a}_2 = \frac{a}{2}\hat{x} + \frac{\sqrt{3}a}{2}\hat{y}$, the reciprocal lattice basis vectors are

$$\mathbf{b}_1 = \frac{2\pi}{a}\hat{x} - \frac{2\pi}{\sqrt{3}a}\hat{y}, \quad \mathbf{b}_2 = \frac{4\pi}{\sqrt{3}a}\hat{y}. \quad (5)$$

Since our model possesses inversion symmetry, we will calculate the eigenvalues of the parity operator at the four time-reversal-invariant points in k space,¹¹ that is,

$$\mathbf{b} = \frac{n_1}{2}\mathbf{b}_1 + \frac{n_2}{2}\mathbf{b}_2, \quad (6)$$

where

$$n_1, n_2 = 0, 1. \quad (7)$$

From the eigenvalues of the parity operator at the time-reversal-invariant momenta, the Z_2 topological class can be determined as¹¹

$$(-1)^{\nu} = \prod_{a=1}^4 \delta_a, \quad (8)$$

where

$$\delta_a = \prod_{m=1}^N \xi_{2m}(\Gamma_a). \quad (9)$$

Here ν is the Z_2 topological invariant, Γ_a is one of the four time-reversal-invariant points defined as above, and $\xi_{2m}(\Gamma_a)$ is the eigenvalue of the parity operator for the Bloch wave function of the $2m$ th occupied band at the time-reversal-invariant point Γ_a .

Because of the large parameter space of the model, we must choose different “cuts” of the parameters to explore the phase diagrams. We will use the methods described above to determine the phases at filling fractions for different hopping values.

A. Phase diagrams for $t_2 = t_3$

We begin by fixing the second-neighbor hopping values $t_2 = t_3 = \lambda_{SO}$ in (3). Thus we take uniform spin-orbit coupling λ_{SO} and inter-triangle hopping t_1 as tuning parameters which are expected to drive the system into different phases. Figure 4 depicts the phase diagrams for filling fractions $1/6$, $1/3$, $1/2$, $2/3$, and $5/6$. (In the figure, and all related figures that follow in the paper the gray-scale coding is as follows: black = conductor, gray = insulator, and white = topological insulator.)

A variety of phases are seen at different fillings. Starting with $1/6$ filling, we see that the middle axis $\lambda_{SO} = 0$ is never in the topological insulator phase. This is easy to understand because in the absence of spin-orbit coupling, the system can only be a metal or trivial insulator. There

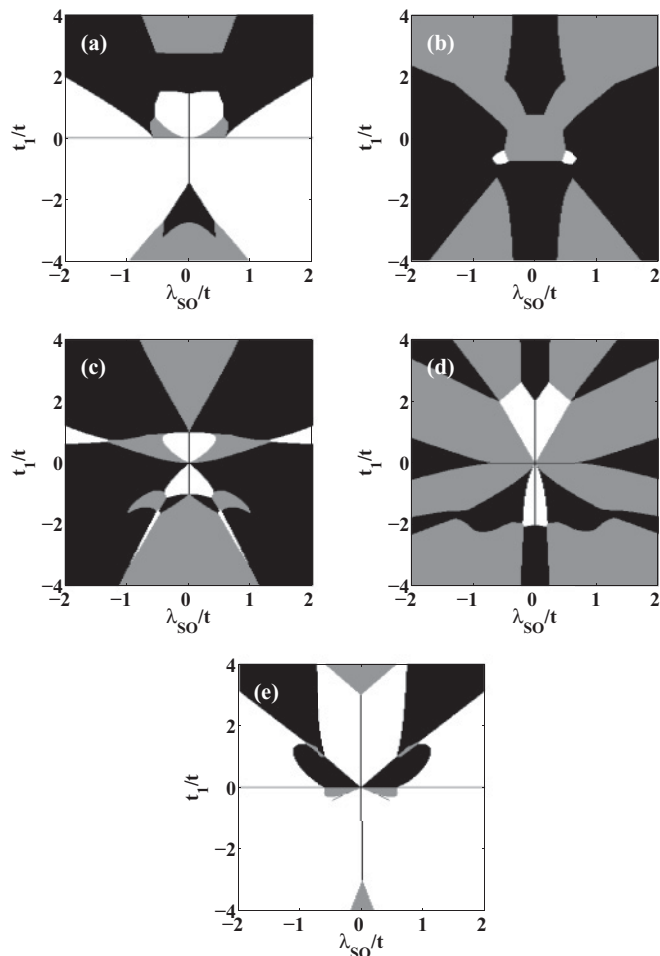


FIG. 4. Phase diagrams for different filling fractions. Figures (a)–(e) are for the filling fraction from $1/6$ to $5/6$, with filling fraction increasing in units of $1/6$. For each filling, the vertical and horizontal axes measure t_1 and $t_2 = t_3 = \lambda_{SO}$, in units of t , respectively. The gray-scale coding is as follows: black = conductor, gray = insulator, and white = topological insulator.

also exists a horizontal straight line on the phase diagram which corresponds to the metallic phase when the inter-triangle hopping is zero. It is noteworthy that large areas of the phase diagram are occupied by the topological insulator. That is consistent with the observation of Dirac points at $1/6$ filling for $t_2 = t_3 = 0$ in the bulk energy bands and the crossing edge modes on the strip geometry for $\lambda_{SO} \neq 0$. The phenomenology is similar to the case of the decorated honeycomb lattice model.⁶⁶

At $1/3$ filling most areas are either a conductor or a trivial insulator, which is consistent with the lack of Dirac cones or quadratically touching points in the bulk energy bands when there is no spin-orbit coupling. However, as the spin-orbit coupling is turned on, at some special parameters the system can still be a topological insulator, as shown by white spots in Fig. 4(b).

At $1/2$ filling the phase diagram appears rather complex. In most areas it is a conductor, while for some areas the trivial insulator and the topological insulator can be distinguished. The topological insulator phase also appears on some narrow areas close to the region around $\lambda_{SO} = \pm 0.7t$ and $t_1 = -2.0t$.

The phase diagram for $2/3$ filling consists mainly of the trivial insulator and the metallic phase. Nevertheless, small regions around the center of the phase diagram occurring at small values of spin-orbit coupling present the topological insulator phase. For much of the phase diagram, the conducting and trivial insulating phases occur alternately when the hopping strength and/or spin-orbit coupling are increased. The crossing states at $k = 0$ in the calculation on the strip geometry shown in Fig. 3 lies in the narrow region of the topological insulating phase.

Finally, for $5/6$ filling most of the area is occupied by the topological insulator, in strong contrast to the former cases. This is also clearly seen from the calculation in the strip geometry shown in Fig. 3 combined with the less stable quadratic band touching points^{67,83} (compared to Dirac points) that are clearly seen at $5/6$ filling in Fig. 2(a) at the Γ point.

B. Phase diagrams for fixed t_1

As we emphasized earlier, the model (3) supports two types of spin-orbit couplings: t_2 and t_3 . In this section we investigate the interplay between these couplings and the resulting phases. We describe phase diagrams with the same gray-scale coding as before: black = conductor, gray = insulator, and white = topological insulator. We assume that the hopping between triangles, t_1 , is set to a fixed value, and the spin-orbit coupling t_2 and t_3 are independently varied. This type of phase diagram takes a slice in the three-dimensional parameter space $(t_1/t, t_2/t, t_3/t)$. Such phase diagrams reveal even more features than those presented earlier with $t_2 = t_3$ (Fig. 4). In particular, we find that the two second-neighbor spin-orbit coupling terms can “compete” with each other and drive the system out of the topological insulator phase, even though each individually would place it there.

We consider two cases: $t_1 = 0$ and $t_1 = t$. The corresponding phase diagrams are shown in Figs. 5 and 6. The phase diagrams illustrated in Fig. 5 in which $t_1 = 0$ are a special case. First note that in the absence of second-neighbor hopping it is clear the model must be in a trivial insulator phase since the only hopping is around triangular plaquettes in the lattice. Thus, the origin at all filling fractions is a trivial insulator. However, away from the origin the behavior is rather different at different filling fractions. For example, close to the origin the model is in a trivial insulating state at $1/3$ filling, while it remains a metal nearby at $2/3$ filling (for the most part). Interestingly, at $1/6$ filling only the metallic phase appears. Also, at $1/2$ and $5/6$ filling the phase diagram is mostly metallic.

In Fig. 6 we show the phase diagrams for $t_1 = t$. Although those phase diagrams show a complex evolution with the hopping parameters, we can still draw some clear conclusions from them. For example, filling fractions $1/6$ and $5/6$ are rich in regions of topological insulator, while filling fractions $1/3$ and $2/3$ are poor in regions of topological insulator. Filling fraction $1/2$ tends to have roughly one-third to one-half of the parameter space occupied by the topological insulator phase. Ultimately, the explanation for these behaviors comes from the band structure in the presence of second-neighbor hopping. However, as shown in Fig. 2(a), the bands at filling fraction $1/6$ and $2/3$ both have a Dirac cone at the K point so the naive

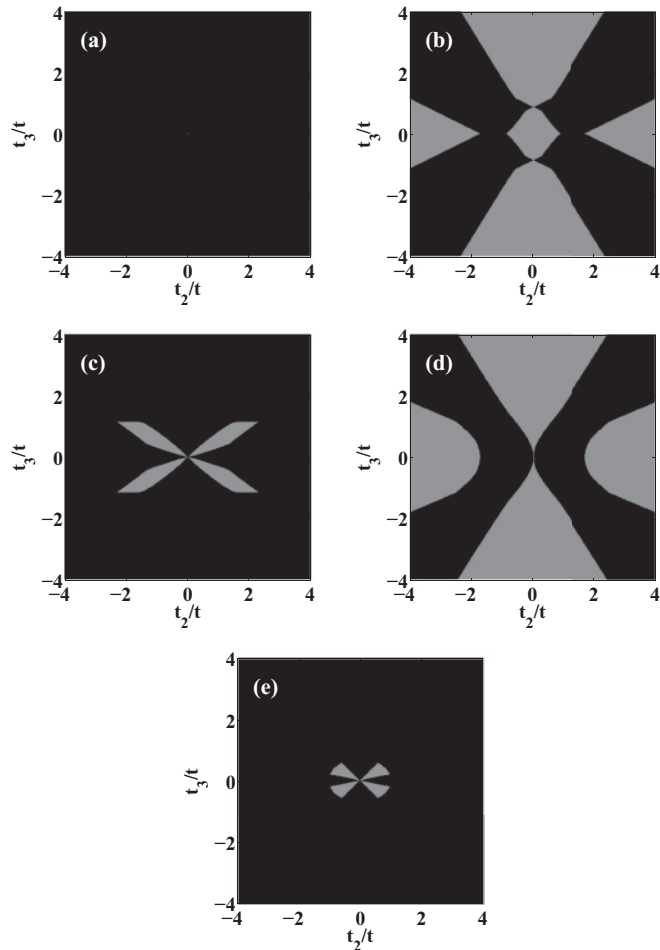


FIG. 5. Phase diagrams for $t_1 = 0$. The horizontal axis is t_2/t , and the vertical axis is t_3/t . Figures (a)–(e) are for the filling fraction from $1/6$ to $5/6$, increasing in units of $1/6$. For all fillings the origin $t_2 = t_3 = 0$ is a trivial insulator.

expectation might be for these two fillings to respond similarly when second-neighbor spin-orbit couplings are added. Our calculations clearly indicate this is not the case and the actual evolution is rather complicated. This feature should be borne in mind when viewing the present model as the result of a self-consistent Hamiltonian in which spin-orbit coupling was spontaneously generated from interactions.^{67,71–74} We note that if the signs of any two among t_1 , t_2 , and t_3 are reversed, the figures show the phase of the system is unchanged. For example, if one flips the phase diagram for $t_1 = t$ (see Fig. 6) around the axis $t_2 = 0$ or $t_3 = 0$, the phase diagram obtained is identical to the phase diagram for the case $t_1 = -t$. This symmetry is easy to verify from the Hamiltonian (1). Indeed, the sign of t_1 can be absorbed via a simple gauge transformation of electron operators. The latter is defined as follows: $c^\dagger(c) \rightarrow -c^\dagger(-c)$ for up triangles and $c^\dagger(c) \rightarrow c^\dagger(c)$ for down triangles. This transformation flips the signs of t_1 and t_3 . Thus this simple argument implies that the phase diagram is symmetric via such transformations. Moreover, if the signs of t_2 and t_3 are flipped, the phase diagram will not change, which can be simply understood by noting that this flipping can also be absorbed into the magnetic fields for different spin species, i.e. $v_{ij} \rightarrow -v_{ij}$.

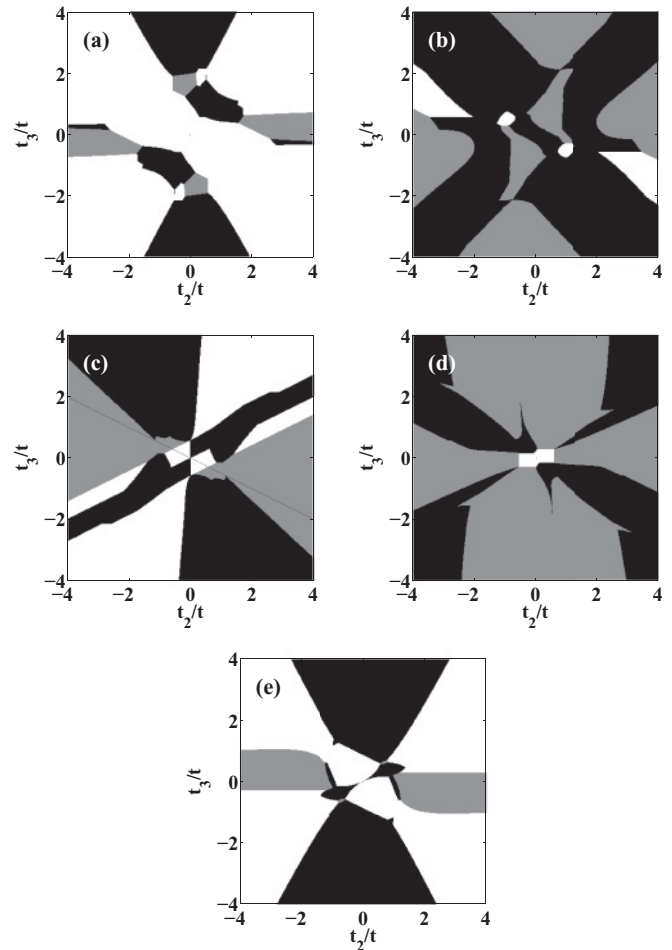


FIG. 6. Phase diagrams for $t_1 = t$. The horizontal axis is t_2/t , and the vertical axis is t_3/t . Figures (a)–(e) are for the filling fraction from $1/6$ to $5/6$, increasing in units of $1/6$.

We also studied other cases with different values of inter-triangle hopping. For example, when $t_1 = 2t$ and the filling fraction is $5/6$, if $t_2 = t$ and $t_3 = 0$, or $t_2 = 0$ and $t_3 = 0.4t$, the system is topological insulating, while if $t_2 = t$ and $t_3 = 0.4t$, the system is a metal (See Fig. 7). A possible explanation for such phenomena is the inner magnetic field created by the two different types of spin-orbit coupling may have opposite contributions to the phase of the hopping terms, and therefore they may cancel each other for some parameter values. A similar inverse case also exists where a single type of spin-orbit coupling does not result in the topological insulator phase while if both types of spin-orbit coupling are present, the system becomes a topological insulator.

IV. FLAT-BAND FRACTIONAL QUANTUM HALL EFFECT

In recent years, lattice models with flat bands have attracted attention for a number of reasons, among them are enhanced interaction effects.^{84–89} Since the scale of the kinetic energy is set by the band width, if the band width vanishes, any residual interparticle interactions will be “large” and may drive the system into a strongly correlated state such as a Wigner crystal⁸⁷ or a fractional quantum Hall state.⁸⁹

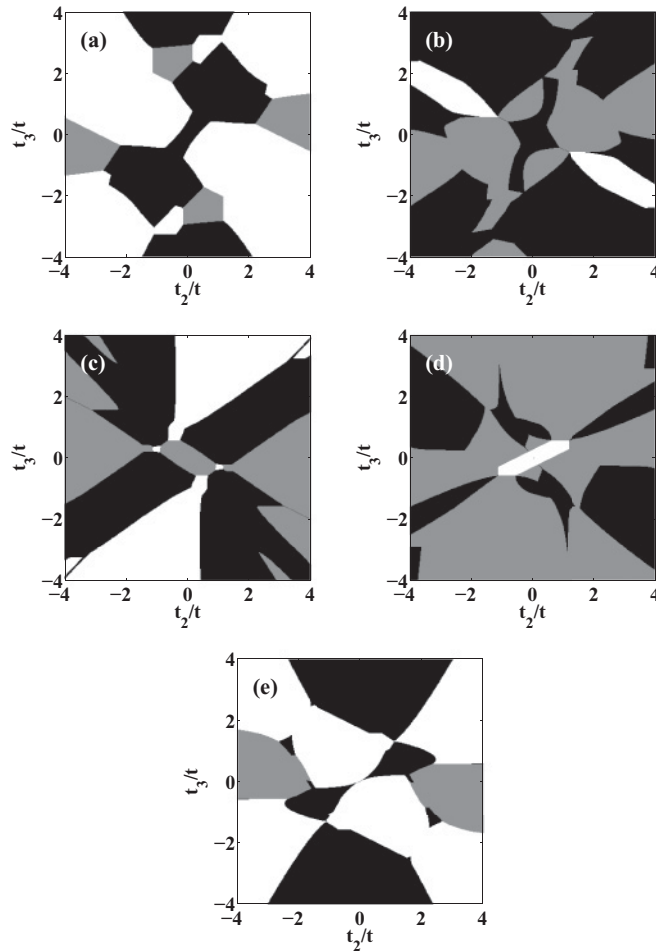


FIG. 7. Phase diagrams for $t_1 = 2t$. The horizontal axis is t_2/t , and the vertical axis is t_3/t . Figures (a)–(e) are for the filling fraction from $1/6$ to $5/6$, increasing in units of $1/6$.

Flat-band lattice models in which the flat bands possess a finite Chern number are thought to be excellent candidates for systems that might realize a fractional quantum Hall effect when the flat band is partially filled.^{76–79} Indeed, exact diagonalization studies on the checkerboard lattice^{75,79} and other lattices^{77,79} support the development of a fractional quantum Hall state at certain filling fractions.

In order to maximize the effectiveness of the interactions in driving a fractional quantum Hall state, the flat band should be as flat as possible *and* the band gap to the next band should be as large as possible. (Virtual transitions to higher lying bands with finite Chern numbers are more effective at disrupting the fractional quantum Hall state than those with zero Chern number.) If we call the bandwidth of the flat band W and the energy difference between the lowest point of the band above the flat band and the highest point of the flat band E_g , the figure of merit is E_g/W , and this should be much larger than unity. If the characteristic strength of the interparticle interactions is U , the regime $W \ll U \ll E_g$ will involve little mixing from the higher bands and the physics will be dominated by the interactions in the flat band with a finite Chern number.

In this section, we show that the ruby lattice possesses flat bands with finite Chern number. One can readily reach the regime $E_g/W \approx 70$.

We first study a new model without the spin-orbit coupling in Eq. (3), but with the imaginary part on the hopping terms from Eq. (2). Specifically, in the Hamiltonian (2) the hopping terms are substituted by

$$t' = t + i\sigma_z t_i, \quad t'_1 = t_{1r} + i\sigma_z t_{1i}. \quad (10)$$

The complex hopping parameters above can be artificially synthesized in fermionic cold atomic optical lattices via a specific tuning of Raman fields,^{90–92} or they can arise in some spin-orbital perovskites where strong intrinsic spin-orbit coupling can make the hopping complex and spin-dependent.⁹³

To explicitly break time-reversal symmetry, we assume the fermions are spin polarized and calculate the band structure and Chern number for one spin orientation. The Chern number of the n th band is defined as⁷⁸

$$c_n = \frac{1}{2\pi} \int_{BZ} d^2k F_{12}(k), \quad (11)$$

where the integral is taken for the two-dimensional Brillouin zone, and $F_{12}(k)$ is the associated field strength defined as

$$F_{12}(k) = \frac{\partial}{\partial k_1} A_2(k) - \frac{\partial}{\partial k_2} A_1(k), \quad (12)$$

where $A_\mu(k) = -i \langle u_{nk} | \frac{\partial}{\partial k_\mu} | u_{nk} \rangle$ is the Berry connection and $|u_{nk}\rangle$ are the Bloch wave functions of the n th band. The full Chern number is the sum of c_n over all occupied bands, which in our case is just the single lowest energy band. The calculation of Chern numbers is based on the methods in Ref. 94, where $F_{12}(k)$ is expressed in some $U(1)$ gauge transformation link variables, and then the integration is converted into a summation in k space. With only the hopping parameters (10) our flattest band with finite Chern number had $W/E_g \approx 13$, which is not very large.

To obtain a nearly flat band with nonzero Chern number, we needed to add more terms to the Hamiltonian. One option is to add the hopping inside the square in the diagonal directions, which is called t_{4r} . This is shown schematically in Fig. 1(c). The nonzero Chern numbers and nearly flat bands do occur in this case. For example, with $t_i = 1.2t$, $t_{1r} = -1.2t$, $t_{1i} = 2.6t$, and $t_{4r} = -1.2t$ the Chern number is -1 , the gap = $2.398t$, and the band width = $0.037t$, which gives $W/E_g \approx 70$. The corresponding band structure is shown in Fig. 8. Based on the results of exact diagonalization studies on other lattices^{75,77,79} and the general arguments given before,^{76–79} we expect a flat-band fractional quantum Hall effect to be realized

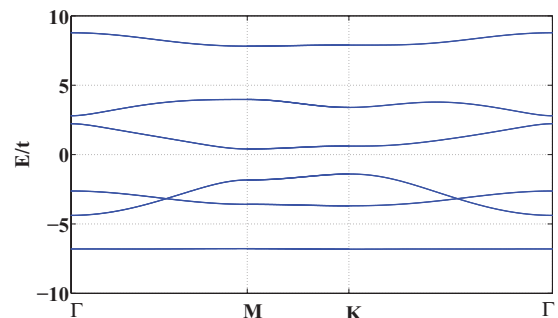


FIG. 8. (Color online) The energy bands with $t_i = 1.2t$, $t_{1r} = -1.2t$, $t_{1i} = 2.6t$, and $t_{4r} = -1.2t$.

on the ruby lattice as well for the appropriate fractional filling of the flat band. This could form the basis of a lattice model of a fractional topological insulator⁹⁵ by taking two time-reversed copies.^{62,63}

V. CONCLUSION

In conclusion, we have studied the energy bands of a tight-binding model on the ruby lattice, and we also obtained the phase diagrams for a variety of filling fractions. The phase diagram is rather complex in its dependence on the various types of spin-orbit coupling and nearest-neighbor hopping we considered. We have seen how various spin-orbit coupling terms can “compete” with each other and also “support” each other.

In a related spinless model we calculated the Chern number for the nearly flat bands, and we showed that they will likely support a robust fractional quantum Hall effect with $W/E_g \approx 70$. This could lead to possible lattice models of a fractional topological insulator.⁹⁵

Since the ruby lattice has earlier appeared in the study of topological spin models,^{60,61} the current work opens the way for an exploration of the transitions among various interesting phases in a more general interacting model.⁹⁶ Current technology in cold atomic gases should allow an experimental study^{97–103} (although perhaps with challenges) of fermions in the ruby lattice and will likely raise new questions to challenge theory.

ACKNOWLEDGMENTS

We thank Jun Wen for helpful discussions, and we gratefully acknowledge funding from ARO Grant No. W911NF-09-1-0527 and NSF Grant No. DMR-0955778. The authors acknowledge the Texas Advanced Computing Center (TACC) at The University of Texas at Austin for providing computing resources that have contributed to the research results reported within this paper. URL: <http://www.tacc.utexas.edu>

*phyxiang@gmail.com

¹X.-G. Wen, *Quantum Field Theory of Many-Body Systems* (Oxford University Press, New York, 2004).

²G. E. Volovik, *The Universe in a Helium Droplet* (Clarendon, Oxford, 2003).

³C. Nayak, S. H. Simon, A. Stern, M. Freedman, and S. Das Sarma, *Rev. Mod. Phys.* **80**, 1083 (2008).

⁴M. Levin and X.-G. Wen, *Phys. Rev. Lett.* **96**, 110405 (2006).

⁵J. Eisert, M. Cramer, and M. B. Plenio, *Rev. Mod. Phys.* **82**, 277 (2010).

⁶L. Amico, R. Fazio, A. Osterloh, and V. Vedral, *Rev. Mod. Phys.* **80**, 517 (2008).

⁷X.-L. Qi and S.-C. Zhang, *Phys. Today* **63**, 33 (2010).

⁸J. E. Moore, *Nature (London)* **464**, 194 (2010).

⁹M. Z. Hasan and C. L. Kane, *Rev. Mod. Phys.* **82**, 3045 (2010).

¹⁰B. A. Bernevig, T. L. Hughes, and S.-C. Zhang, *Science* **314**, 1757 (2006).

¹¹L. Fu and C. L. Kane, *Phys. Rev. B* **76**, 045302 (2007).

¹²J. C. Y. Teo, L. Fu, and C. L. Kane, *Phys. Rev. B* **78**, 045426 (2008).

¹³H. Zhang, C.-X. Liu, X.-L. Qi, X. Dai, Z. Fang, and S.-C. Zhang, *Nat. Phys.* **5**, 438 (2009).

¹⁴S. Chadov, X.-L. Qi, J. Kübler, G. H. Fecher, C. Felser, and S.-C. Zhang, *Nat. Mater.* **9**, 541 (2010).

¹⁵J. Wang, R. Li, S.-C. Zhang, and X.-L. Qi, *Phys. Rev. Lett.* **106**, 126403 (2011).

¹⁶W. Feng, D. Xiao, J. Ding, and Y. Yao, *Phys. Rev. Lett.* **106**, 016402 (2011).

¹⁷H.-J. Zhang, S. Chadov, L. Müchler, B. Yan, X.-L. Qi, J. Kübler, S.-C. Zhang, and C. Felser, *Phys. Rev. Lett.* **106**, 156402 (2011).

¹⁸D. Xiao, Y. Yao, W. Feng, J. Wen, W. Zhu, X.-Q. Chen, G. M. Stocks, and Z. Zhang, *Phys. Rev. Lett.* **105**, 096404 (2010).

¹⁹H. Lin, R. S. Markiewicz, L. A. Wray, L. Fu, M. Z. Hasan, and A. Bansil, *Phys. Rev. Lett.* **105**, 036404 (2010).

²⁰Y. L. Chen *et al.*, *Phys. Rev. Lett.* **105**, 266401 (2010).

²¹B. Yan, C.-X. Liu, H.-J. Zhang, C.-Y. Yam, X.-L. Qi, T. Frauenheim, and S.-C. Zhang, *Europhys. Lett.* **90**, 37002 (2010).

²²B. Yan, H.-J. Zhang, C.-X. Liu, X.-L. Qi, T. Frauenheim, and S.-C. Zhang, *Phys. Rev. B* **82**, 161108 (2010).

²³H. Lin, L. Wray, Y. Xia, S.-Y. Xu, S. Jia, R. Cava, A. Bansil, and M. Hasan, e-print arXiv:1004.0999.

²⁴B. Yan, L. Mchler, X.-L. Qi, S.-C. Zhang, and C. Felser, e-print arXiv:1104.0641.

²⁵H. Lin, L. Wray, Y. Xia, S. Jia, R. Cava, A. Bansil, and M. Hasan, *Nat. Mater.* **9**, 546 (2010).

²⁶Y. Sun, X.-Q. Chen, S. Yunoki, D. Li, and Y. Li, *Phys. Rev. Lett.* **105**, 216406 (2010).

²⁷W. Feng, D. Xiao, Y. Zhang, and Y. Yao, *Phys. Rev. B* **82**, 235121 (2010).

²⁸W. Al-Sawai, H. Lin, R. S. Markiewicz, L. A. Wray, Y. Xia, S.-Y. Xu, M. Z. Hasan, and A. Bansil, *Phys. Rev. B* **82**, 125208 (2010).

²⁹M. König, S. Wiedmann, C. Brune, A. Roth, H. Buhmann, L. Molenkamp, X.-L. Qi, and S.-C. Zhang, *Science* **318**, 766 (2007).

³⁰A. Roth, C. Brüne, H. Buhmann, L. W. Molenkamp, J. Maciejko, X.-L. Qi, and S.-C. Zhang, *Science* **325**, 294 (2009).

³¹D. Hsieh, D. Qian, L. Wray, Y. Xia, Y. Hor, R. J. Cava, and M. Z. Hasan, *Nature (London)* **452**, 970 (2008).

³²D. Hsieh *et al.*, *Science* **323**, 919 (2009).

³³Y. Xia *et al.*, *Nat. Phys.* **5**, 398 (2009).

³⁴Y. L. Chen *et al.*, *Science* **325**, 178 (2009).

³⁵D. Hsieh *et al.*, *Nature (London)* **460**, 1101 (2009).

³⁶D. Hsieh *et al.*, *Phys. Rev. Lett.* **103**, 146401 (2009).

³⁷Y. S. Hor, A. Richardella, P. Roushan, Y. Xia, J. G. Checkelsky, A. Yazdani, M. Z. Hasan, N. P. Ong, and R. J. Cava, *Phys. Rev. B* **79**, 195208 (2009).

³⁸T. Sato, K. Segawa, H. Guo, K. Sugawara, S. Souma, T. Takahashi, and Y. Ando, *Phys. Rev. Lett.* **105**, 136802 (2010).

³⁹K. Kuroda *et al.*, *Phys. Rev. Lett.* **105**, 146801 (2010).

⁴⁰A. Nishide, A. A. Taskin, Y. Takeichi, T. Okuda, A. Kakizaki, T. Hirahara, K. Nakatsuji, F. Komori, Y. Ando, and I. Matsuda, *Phys. Rev. B* **81**, 041309 (2010).

- ⁴¹A. P. Schnyder, S. Ryu, A. Furusaki, and A. W. W. Ludwig, *Phys. Rev. B* **78**, 195125 (2008).
- ⁴²R. Roy, *Phys. Rev. B* **79**, 195321 (2009).
- ⁴³R. Roy, *Phys. Rev. B* **79**, 195322 (2009).
- ⁴⁴J. E. Moore and L. Balents, *Phys. Rev. B* **75**, 121306 (2007).
- ⁴⁵L. Fu, C. L. Kane, and E. J. Mele, *Phys. Rev. Lett.* **98**, 106803 (2007).
- ⁴⁶C. Wu, B. A. Bernevig, and S.-C. Zhang, *Phys. Rev. Lett.* **96**, 106401 (2006).
- ⁴⁷C. Xu and J. E. Moore, *Phys. Rev. B* **73**, 045322 (2006).
- ⁴⁸A. Ström and H. Johannesson, *Phys. Rev. Lett.* **102**, 096806 (2009).
- ⁴⁹C.-Y. Hou, E.-A. Kim, and C. Chamon, *Phys. Rev. Lett.* **102**, 076602 (2009).
- ⁵⁰C. Xu and L. Fu, *Phys. Rev. B* **81**, 134435 (2010).
- ⁵¹J. C. Y. Teo and C. L. Kane, *Phys. Rev. B* **79**, 235321 (2009).
- ⁵²K. T. Law, C. Y. Seng, P. A. Lee, and T. K. Ng, *Phys. Rev. B* **81**, 041305 (2010).
- ⁵³V. A. Zyuzin and G. A. Fiete, *Phys. Rev. B* **82**, 113305 (2010).
- ⁵⁴Y. Tanaka and N. Nagaosa, *Phys. Rev. Lett.* **103**, 166403 (2009).
- ⁵⁵J. Maciejko, C. Liu, Y. Oreg, X.-L. Qi, C. Wu, and S.-C. Zhang, *Phys. Rev. Lett.* **102**, 256803 (2009).
- ⁵⁶X.-L. Qi, T. L. Hughes, and S.-C. Zhang, *Phys. Rev. B* **78**, 195424 (2008).
- ⁵⁷X.-L. Qi, J. Zang, and S.-C. Zhang, *Science* **323**, 1184 (2009).
- ⁵⁸A. M. Essin, J. E. Moore, and D. Vanderbilt, *Phys. Rev. Lett.* **102**, 146805 (2009).
- ⁵⁹A. M. Essin, A. M. Turner, J. E. Moore, and D. Vanderbilt, *Phys. Rev. B* **81**, 205104 (2010).
- ⁶⁰H. Bombin, M. Kargarian, and M. A. Martin-Delgado, *Phys. Rev. B* **80**, 075111 (2009).
- ⁶¹M. Kargarian, H. Bombin, and M. Martin-Delgado, *New J. Phys.* **12**, 025018 (2010).
- ⁶²C. L. Kane and E. J. Mele, *Phys. Rev. Lett.* **95**, 146802 (2005).
- ⁶³C. L. Kane and E. J. Mele, *Phys. Rev. Lett.* **95**, 226801 (2005).
- ⁶⁴F. D. M. Haldane, *Phys. Rev. Lett.* **61**, 2015 (1988).
- ⁶⁵B. A. Bernevig and S.-C. Zhang, *Phys. Rev. Lett.* **96**, 106802 (2006).
- ⁶⁶A. Rüegg, J. Wen, and G. A. Fiete, *Phys. Rev. B* **81**, 205115 (2010).
- ⁶⁷K. Sun, H. Yao, E. Fradkin, and S. A. Kivelson, *Phys. Rev. Lett.* **103**, 046811 (2009).
- ⁶⁸M. Kargarian and G. A. Fiete, *Phys. Rev. B* **82**, 085106 (2010).
- ⁶⁹H.-M. Guo and M. Franz, *Phys. Rev. B* **80**, 113102 (2009).
- ⁷⁰C. Weeks and M. Franz, *Phys. Rev. B* **82**, 085310 (2010).
- ⁷¹S. Raghu, X.-L. Qi, C. Honerkamp, and S.-C. Zhang, *Phys. Rev. Lett.* **100**, 156401 (2008).
- ⁷²J. Wen, A. Rüegg, C.-C. J. Wang, and G. A. Fiete, *Phys. Rev. B* **82**, 075125 (2010).
- ⁷³Y. Zhang, Y. Ran, and A. Vishwanath, *Phys. Rev. B* **79**, 245331 (2009).
- ⁷⁴Q. Liu, H. Yao, and T. Ma, *Phys. Rev. B* **82**, 045102 (2010).
- ⁷⁵D. N. Sheng, Z.-C. Gu, K. Sun, and L. Sheng, *Nat. Commun.* **2**, 389 (2011).
- ⁷⁶K. Sun, Z. Gu, H. Katsura, and S. Das Sarma, *Phys. Rev. Lett.* **106**, 236803 (2011).
- ⁷⁷T. Neupert, L. Santos, C. Chamon, and C. Mudry, *Phys. Rev. Lett.* **106**, 236804 (2011).
- ⁷⁸E. Tang, J.-W. Mei, and X.-G. Wen, *Phys. Rev. Lett.* **106**, 236802 (2011).
- ⁷⁹Y.-F. Wang, Z.-C. Gu, C.-D. Gong, and D. N. Sheng, e-print arXiv:1103.1686.
- ⁸⁰L. Fu, *Phys. Rev. Lett.* **103**, 266801 (2009).
- ⁸¹L. Fu, *Phys. Rev. Lett.* **106**, 106802 (2011).
- ⁸²For a description of the differential evolution method see [<http://www.nehu-economics.info/difevol.html>].
- ⁸³F. Zhang, J. Jung, G. A. Fiete, Q. Niu, and A. H. MacDonald, *Phys. Rev. Lett.* **106**, 156801 (2011).
- ⁸⁴K. Ohgushi, S. Murakami, and N. Nagaosa, *Phys. Rev. B* **62**, R6065 (2000).
- ⁸⁵D. L. Bergman, C. Wu, and L. Balents, *Phys. Rev. B* **78**, 125104 (2008).
- ⁸⁶Y. Xiao, V. Pelletier, P. M. Chaikin, and D. A. Huse, *Phys. Rev. B* **67**, 104505 (2003).
- ⁸⁷C. Wu, D. Bergman, L. Balents, and S. Das Sarma, *Phys. Rev. Lett.* **99**, 070401 (2007).
- ⁸⁸D. Green, L. Santos, and C. Chamon, *Phys. Rev. B* **82**, 075104 (2010).
- ⁸⁹E. Kapit and E. Mueller, *Phys. Rev. Lett.* **105**, 215303 (2010).
- ⁹⁰K. Osterloh, M. Baig, L. Santos, P. Zoller, and M. Lewenstein, *Phys. Rev. Lett.* **95**, 010403 (2005).
- ⁹¹Y.-J. Lin, R. L. Compton, A. R. Perry, W. D. Phillips, J. V. Porto, and I. B. Spielman, *Phys. Rev. Lett.* **102**, 130401 (2009).
- ⁹²I. B. Spielman, *Phys. Rev. A* **79**, 063613 (2009).
- ⁹³A. Shimoyamada *et al.*, *Phys. Rev. Lett.* **96**, 026403 (2006).
- ⁹⁴T. Fukui, Y. Hatsugai, and H. Suzuki, *J. Phys. Soc. Jpn.* **74**, 1674 (2005).
- ⁹⁵M. Levin and A. Stern, *Phys. Rev. Lett.* **103**, 196803 (2009).
- ⁹⁶G. A. Fiete *et al.*, e-print arXiv:1106.0013.
- ⁹⁷A. S. Sørensen, E. Demler, and M. D. Lukin, *Phys. Rev. Lett.* **94**, 086803 (2005).
- ⁹⁸M. Hafezi, A. S. Sørensen, E. Demler, and M. D. Lukin, *Phys. Rev. A* **76**, 023613 (2007).
- ⁹⁹L.-M. Duan, E. Demler, and M. D. Lukin, *Phys. Rev. Lett.* **91**, 090402 (2003).
- ¹⁰⁰J. Ruostekoski, *Phys. Rev. Lett.* **103**, 080406 (2009).
- ¹⁰¹D. Bercioux, D. F. Urban, H. Grabert, and W. Häusler, *Phys. Rev. A* **80**, 063603 (2009).
- ¹⁰²D. Bercioux, N. Goldman, and D. F. Urban, *Phys. Rev. A* **83**, 023609 (2011).
- ¹⁰³N. Goldman, D. F. Urban, and D. Bercioux, *Phys. Rev. A* **83**, 063601 (2011).